



HHS Public Access

Author manuscript

Biomacromolecules. Author manuscript; available in PMC 2024 March 08.

Published in final edited form as:

Biomacromolecules. 2024 February 12; 25(2): 690–699. doi:10.1021/acs.biomac.3c00911.

Neutron Scattering Analysis of *Cryptococcus neoformans* Polysaccharide Reveals Solution Rigidity and Repeating Fractal-like Structural Patterns

Ziwei Wang¹, Susana C. M. Teixeira^{2,3,*}, Camilla Strother¹, Anthony Bowen¹, Arturo Casadevall¹, Radamés JB Cordero^{1,*}

¹Department of Molecular Microbiology and Immunology, Johns Hopkins Bloomberg School of Public Health, Baltimore, Maryland, 21205, USA

²NIST Center of Neutron Research, National Institute of Standards and Technology, Gaithersburg, Maryland, 20899, USA

³Department of Chemical and Biomolecular Engineering, University of Delaware, Newark, Delaware, 19716, USA

Abstract

Cryptococcus neoformans is a fungal pathogen that can cause life-threatening brain infections in immunocompromised individuals. Unlike other fungal pathogens, it possesses a protective polysaccharide capsule that is crucial for its virulence. During infections, *Cryptococcus* cells release copious amounts of extracellular polysaccharides (exo-PS) that interfere with host immune responses. Both exo-PS and capsular-PS play pivotal roles in *Cryptococcus* infections and serve as essential targets for disease diagnosis and vaccine development strategies. However, understanding their structure is complicated by their polydispersity, complexity, sensitivity to sample isolation and processing, and scarcity of methods capable of isolating and analyzing them while preserving their native structure. In this study, we employ small-angle neutron scattering (SANS) and ultra-small angle neutron scattering (USANS) for the first time to investigate both fungal cell suspensions and extracellular polysaccharides in solution. Our data suggests that exo-PS in solution exhibits collapsed chain-like behavior and demonstrates mass fractal properties that indicate a relatively condensed pore structure in aqueous environments. This observation is also supported by scanning electron microscopy (SEM). The local structure of the polysaccharide is characterized as a rigid rod, with a length-scale corresponding to 3 to 4 repeating units. This research not only unveils insights into exo-PS and capsular-PS structures but also demonstrates the

* **Corresponding Authors:** rcorder4@jhu.edu. susanat@udel.edu.

Author Contributions

RJBC and SCMT designed the neutron scattering experimental approach. CS and RJBC designed the cell culture and polysaccharide isolation protocols, prepared samples, and collected optical microscopy data. SCMT and CS collected and reduced the neutron scattering data. SCMT and ZW carried out the data fitting and analyses. AB carried out the fractal dimension analysis on SEM images. The manuscript was written through the contributions of all authors. All authors have approved the final version of the manuscript.

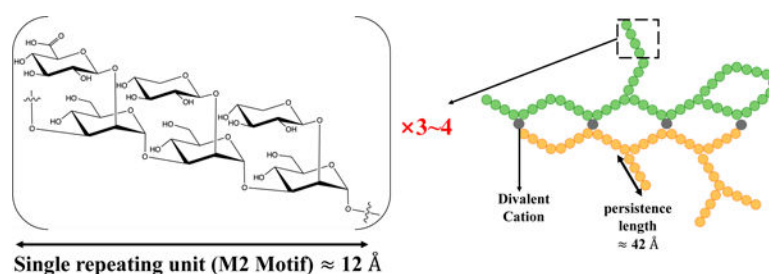
ASSOCIATED CONTENT

Supporting Information: dynamic light scattering analysis of exo-PS, neutron, and X-ray scattering data and data fitting for exo-PS samples, microscopy data for whole cell samples, and Guinier fittings and Kratky plots for the fungal cell samples based on USANS and SANS data, respectively (PDF).

The authors declare no competing financial interest.

potential of USANS for studying changes in cell dimensions and the promise of contrast variation in future neutron scattering studies.

Graphical Abstract



BRIEFS

For Table of Content (TOC) only; a graphic reflecting the characteristics of the *Cryptococcus* exo-PS.

Keywords

Cryptococcus ; extracellular polysaccharide; neutron scattering; glucuronoxylomannan; mass fractal; fungal pathogen

INTRODUCTION

Cryptococcal meningitis is a deadly fungal infection caused by *Cryptococcus neoformans*, one of the leading causes of death in HIV/AIDS patients in sub-Saharan Africa^{1,2}. Within brain tissues, the fungus secretes copious amounts of polysaccharide (exo-PS) to the cerebrospinal fluid, believed to cause elevated intracranial pressure and disruption of an effective immune response^{2,3}. The fungal cell is encased by a thick capsule composed of polysaccharide (capsular-PS), which protects from the host's immune defense mechanisms⁴. Both the exo-PS and capsular-PS are mainly comprised of glucuronoxylomannan (GXM), which is formed by an α -1,3-linked mannan backbone with β -1,2-linked glucuronic acid and β -1,2- or β -1,4-linked xylose as its branching residues that contribute to serological diversity. GXM molecules are assembled from six structural units (M1-6), referred to as triads, featuring a glucuronic acid residue every third mannose along with varying xylose substitutions (Figure 1). Due to its high water-content (over 95% of total mass and volume), the PS capsule is highly susceptible to the dehydration steps employed in high-resolution microscopy or lyophilization, which disturbs the native structure^{5,6}.

C. neoformans exo-PS and capsular-PS are key virulence determinants and targets for the immune system, vaccine design, and monoclonal antibody (mAb) treatments. Diagnosis of *Cryptococcus* infection primarily relies on culturing the organism and antigen detection of shed PS^{7,8}. Although both exo-PS and capsular-PS are predominantly composed of GXM, they exhibit distinct physicochemical properties and mAb reactivity⁸. Despite their significance in disease and diagnosis and the known chemical composition of the GXM, the macro- and supramolecular assembly of the *Cryptococcal* PS and the corresponding

effects on epitope binding by antibodies remain largely unknown. Studying the correlation between nanoscale structure and macroscopic properties of the PS, and how both natural and experimental environments can trigger different assembly characteristics, is crucial for the design of diagnostic assays and strategies for vaccine development.

The large and complex PS heteropolymers display physicochemical characteristics that vary based on nutrient availability, chemical and physical environment, and cell age^{8,9}. Consequently, experimental biases can be introduced by sample preparation protocols and the inherent limitations of measurement techniques. Previous research has primarily focused on PS isolated from culture supernatants using hexadecyltrimethylammonium bromide (CTAB) precipitation or filtration, and capsular-PS extracted via dimethylsulfoxide (DMSO) extraction and ionizing radiation-induced PS ablation, leading to nominally de-capsulated cells (residual capsular-PS may remain). A variety of techniques, such as static (SLS) and dynamic light scattering (DLS), zeta potential measurements, optical tweezers-based elastic modulus assessments, and solution viscosity analyses, have been employed to investigate exo-PS and capsular-PS structure^{10,11}. SLS and DLS analyses suggest that the polysaccharide molecules are branched, a characteristic that influences immune reactivity and modulation^{12–15}. Existing experimental data is consistent with capsular-PS polymers in molar mass ranges of 1–7 MDa, radii of gyration (R_g) ranging from 150–500 nm, hydrodynamic radii (R_h) ranging spanning 570–2000 nm, contingent on the specific experimental method used^{10,13,16,17}. Encapsulated and nominally de-capsulated cells were previously investigated by powder X-ray diffraction, where broad peaks in the range of 1.46 \AA^{-1} – 1.51 \AA^{-1} of momentum transfer vector q , were attributed to a repeating structural motif arising from inter-molecular interactions mediated by divalent metals and glucuronic acid residues, and/or possibly gelled PS organization¹⁸. To achieve a detailed characterization of the relationship between the structures of exo-PS and capsular-PS and their corresponding functions at different stages of infection, measurement capabilities that preserve PS conformation are necessary.

In this study, we used neutron scattering analyses, light microscopy, and scanning electron microscopy to probe the structure of exo-PS, intact fungal cells, and gamma-irradiated nominally de-capsulated cells in solution (Figure 2). Neutron scattering accesses a broad range of structural features without causing radiation damage, enabling data collection on the same samples across small-angle (SANS) and ultra-small angle (USANS) neutron scattering regimes at various temperatures and concentrations. This approach has been previously used for studies of polysaccharides, such as arabinoxylans by Yu *et al.*²², and minimizes sample discrepancies, while the use of varying percentages of D₂O in buffers allows for contrast variation. Given the considerable size of the cells (micrometers in diameter), the USANS regime is crucial, whereas the analysis of intrachain structures is conducted within the SANS regime.

MATERIALS AND METHODS

Fungal Growth.

Cryptococcus neoformans Serotype A strain H99 was inoculated in 20 mL of Sabouraud dextrose broth and grown with agitation (120 rpm) for 2 days at 30 °C. The cells were

pelleted by centrifuging for 10 minutes at 3000 rpm, and resuspended in minimal media (15 mM dextrose, 10 mM MgSO₄, 29.3 mM KH₂PO₄, 13 mM glycine, and 3 μM thiamine-HCl, adjusted to pH 5.5 using KOH; where “M” represents the SI unit mol/L). The washing process was repeated three times, and the cells were finally resuspended in minimal media to a density of 1×10⁶ cells/mL. Subsequently, the cells were inoculated into a 1 L culture of minimal media and incubated at 30 °C for 7 days. The cells were harvested via centrifugation at 4,000 rpm for 20 minutes. The supernatant was filtered using a 0.22 μm Millipore.

Capsular-PS was removed by exposing the whole cells to 40 minutes of gamma irradiation, using the method demonstrated by Maxson *et al.*²³. The ionizing radiation was demonstrated to be effective in removing the capsular-PS²⁴.

Exo-PS Isolation.

The exo-PS was isolated from the cell-free supernatant as previously described²⁵. The supernatant was sequentially filtered with an Amicon membrane filter (100 kDa nominal molar mass cutoff) and the flow-through was then filtered using a 10 kDa membrane filter. The exo-PS accumulated on the 10 kDa membrane surface as a clear gel and was collected and dialyzed extensively against MilliQ-grade H₂O or D₂O (Cambridge Isotope Labs, 99.9% D). The H₂O solutions provide scattering profiles at an additional contrast, while the samples prepared in D₂O are expected to minimize the incoherent neutron scattering background contribution to the measured intensity profiles. Following dialysis, the exo-PS concentration was determined using a phenol sulfuric colorimetry assay²⁶. Sample solutions were centrifuged for 2 minutes at 10,000 rpm to remove any debris. This process resulted in 10mg/mL exo-PS samples with a hydrodynamic radius R_h of 550–600 nm and relatively low polydispersity, quantified as 0.355 (Figure S1) by DLS coupled with a 90Plus/BI-MAS Multi-Angle Particle Sizing analyzer (Brookhaven Instruments Corp., NY, USA), as described by Frases *et al.*¹⁶. The prepared exo-PS was also resuspended at 1 mg/mL and 5 mg/mL. Based on the equation derived by Vadillo *et al.*²⁷ ($c^* \approx 1.46/[\eta]$) and the intrinsic viscosity ($[\eta]$) of PS from strain H99 in minimal media determined by Cordero *et al.*¹³, the overlap concentration c^* for exo-PS is estimated as 5 mg/mL²⁸.

SANS and USANS Data Collection and Reduction.

Neutron scattering data were collected at the National Institute of Standards and Technology (NIST) Center for Neutron Research (NCNR; Gaithersburg, Maryland USA). All samples were degassed for 10 minutes before data collection. SANS data were obtained from the 30-meter instruments NG7 and NGB, using a neutron wavelength λ of 6 Å and a wavelength spread $\Delta\lambda/\lambda$ of 12.5 % for three sample-to-detector distances, to measure scattered intensities over a range of momentum transfer defined as:

$$q = \frac{4\pi \sin \theta}{\lambda} \quad (1)$$

where 2θ is the scattering angle measured. Focusing lenses were used for the longer wavelengths (8.4 Å on NGB, and 8.09 Å on NG7) to extend the lower q range to 0.001 \AA^{-1} in the SANS regime²⁹. Scattered neutrons were detected with a 64 cm × 64 cm 2D position-sensitive detector with 128 pixels × 128 pixels at a resolution of 0.508 cm/pixel. SANS data measured for solutions in H₂O at concentrations of exo-PS up to 10 mg/mL show a flat intensity profile in the q range measured, indicative of insufficient contrast to provide a measurable signal above the strong incoherent scattering background from the hydrogen atoms in the buffer (Figure S2). SANS measurements were carried out on 1 mg/mL, 5 mg/mL, and 10 mg/mL of exo-PS solutions in D₂O at three temperatures (22 °C, 30 °C, and 37 °C), controlled by a Peltier-driven sample changer, with 30 minutes of pre-equilibration at the desired temperature before data collection. The temperatures chosen include typical ambient experimental environments (22 °C), as well as the *C. neoformans* optimal growth (30 °C), and physiological temperatures (37 °C). No significant differences were observed between the SANS profiles of exo-PS solutions at the three measured temperatures (data not shown): the profiles overlapped well, within experimental error. A temperature of 30 °C was therefore chosen for data collection on the whole cells and gamma-irradiated cells in the SANS and USANS regime, to maintain consistency with the growth temperature of the whole fungal cells.

Slit-smear USANS data were collected at the double-crystal diffractometer (Bonse-Hart) BT5 at the NCNR ($\lambda = 2.4 \text{ \AA}$, $\lambda/\lambda = 6\%$)³⁰, to cover a q range of 0.00003 \AA^{-1} to 0.003 \AA^{-1} . USANS measurements were carried out on 10 mg/mL exo-PS in D₂O at 30 °C to probe the presence of aggregates or finite size clusters or aggregates in the micrometer to hundreds of nanometers size range. USANS data were also collected on D₂O and H₂O solutions of the whole fungal cells, and gamma irradiated cells at the concentration of 1×10^8 cells/mL.

SANS and USANS data were reduced using the macro-routines developed for IGOR Pro at the NCNR³¹. Raw counts were normalized to a common neutron monitor count and corrected for empty cell counts, ambient background counts, and nonuniform detector response. The data obtained from the samples were placed on an absolute scale by normalizing the scattered intensity to the incident beam flux. Buffer-only reduced data were subtracted from SANS data on samples containing exo-PS or capsular-PS.

Neutron Scattering Data Fitting.

The SANS data for the exo-PS solutions in D₂O were fitted using a modified empirical correlation length function that calculates scattering intensities as:

$$I(q) = \frac{A}{q^n} + \frac{C}{1 + (q\xi)^m} + B \quad (2)$$

where the first term describes Porod scattering from pore clusters (exponent n) and the second term is a Lorentzian function describing scattering from the PS polymer chains (exponent m)³². The second term characterizes the PS/solvent interactions, and the two multiplicative factors A and C are, respectively, the Porod scale and the Lorentz scale.

ξ is a correlation length for the PS chains, and B is a q -independent incoherent neutron scattering intensity background contribution to $I(q)$. The calculated intensities from the correlation length model were smeared to match the instrumental pinhole smearing read from the reduced experimental data file. The exo-PS volume fraction and the B parameter were kept fixed throughout the fits. The fitting parameters and relevant information on the goodness-of-fit are available in the supporting information for the interested reader (Table S1). It was assumed that the entanglement of overlapping PS chains did not contribute significantly towards the SANS profiles.

Light Microscopy.

To measure the cell and capsule dimensions, whole cells and gamma-irradiated cells in D₂O and H₂O at 1×10^8 cells/mL were imaged with an Olympus AX70 microscope, using the QCapture Suite V2.46 software for Windows. *Cryptococcal* cells were suspended in India Ink, which is excluded by the PS so that the capsule region will appear to be bright/empty. Cell dimensions were measured with ImageJ in pixels, and then converted to μm (152 pixels correspond to $50 \mu\text{m}$ for $40\times$ magnification objective with 2×2 binning). Statistical analyses were performed using GraphPad Prism version 9.5.1 for Mac OS X, GraphPad Software, Boston, Massachusetts USA. Unpaired statistical analyses t-tests were done for the cell diameters and capsule thickness comparisons; the corresponding significance was stratified based on the probability that the results occur by chance, quantified as a probability through a percentage p-value, where 5% is equivalent to $p = 0.05$.

Scanning Electron Microscopy.

SEM of encapsulated *C. neoformans* yeast cells was done as previously described¹³. Briefly, the cells were fixed using a solution containing glutaraldehyde, sodium Cacodylate, sucrose, and MgCl₂. After dehydration with ethanol, critical point drying was performed using liquid carbon dioxide. The dried samples were then sputter-coated with gold-palladium for improved conductivity. Finally, the prepared samples were visualized using a JEOL JSM6400 Scanning Electron Microscope at an accelerating voltage of 10 kV, enabling high-resolution imaging of the yeast cells. To analyze the fractal dimension of SEM images of whole cells and capsular-PS structures, we utilized the FracLac plugin of ImageJ (<http://rsb.info.nih.gov/ij/plugins/fracLac/FLHelp/Introduction.htm>). The FracLac algorithm quantifies the complexity of patterns in digital images, providing fractal dimensions data. The algorithm works by scanning the input micrographs using a shifting grid algorithm, which allows multiple scans from different locations on each image.

RESULTS AND DISCUSSION

SANS Analysis of Exo-PS Solutions.

Based solely on the water-free composition, the neutron scattering length density (SLD) of polysaccharides in H₂O is expected to range from $1 \times 10^{-6} \text{ \AA}^{-2}$ to $2 \times 10^{-6} \text{ \AA}^{-2}$ (the SLD of pure H₂O is $-0.56 \times 10^{-6} \text{ \AA}^{-2}$)³³. The flat scattering profiles observed in the exo-PS samples measured in H₂O are consistent with a high hydration state and a significant contribution of incoherent scattering originating from the hydrogen atoms within the samples (Figure S2). In the case of exo-PS solutions in D₂O, there is still a relatively strong incoherent

neutron scattering background observed in the reduced SANS data due to the non-labile hydrogen atoms (Figure 3). The predominant M2 motif expected in our sample consists of three mannoses, two xyloses, and one glucuronic acid²⁰, containing a significant number of labile hydrogens that can exchange against D₂O during dialysis. However, non-labile and solvent-inaccessible hydrogen atoms that remain at varying concentrations are responsible for the differences in background intensities observed at high q in the SANS data for samples at 1 mg/mL, 5 mg/mL, and 10 mg/mL exo-PS (Figure 3).

At low q values, the SANS data for the 10 mg/mL exo-PS in D₂O extend down to 0.001 Å⁻¹ and exhibit a q -dependent intensity profile that reasonably matches the USANS data profile. This indicates the reliability of the desmearing process (a correction applied to the experimental data to account for the slit-smearing effects of the Bonse-Hart USANS instrument) and underscores the consistency between the data collected for the sample in the two scattering regimes³⁴.

For q values below 0.003 Å⁻¹, the SANS scattered intensities of the exo-PS samples at 5 mg/mL and 10 mg/mL display a very similar q^{-n} dependency characteristic of mass fractals (refer to the Porod exponents in Table S1), with $n \approx 2.9$ reflecting a compact gel structure. An increase in inter-cluster interactions is observed for the 5 mg/mL and 10 mg/mL exo-PS solutions, as indicated by the larger Porod scales compared to those at 1 mg/mL exo-PS.

The fitting of the exo-PS SANS data produced a consistent correlation length for all concentrations measured (48.9 ± 7.8 Å for 1 mg/mL exo-PS), which is approximately equivalent to the length of four M2 triads (Figure 4C). The gelation of exo-PS contributes to the viscosity of the solutions and yields a relatively small correlation length³⁵. While the presence of negatively charged glucuronic acid (GlcA) residues can lead to chain-swelling due to electrostatic repulsion, the occurrence of other interactions can stabilize polymer collapse and interchain interactions^{23,36,37}. Namely, hydrogen bonds, van der Waals interactions, and ionic bridging which can be promoted by the presence of the divalent cations Mg²⁺ and Ca²⁺ in the culture media²⁴. The impact of ionic bridging in polysaccharide structure can be observed by the change in the SAXS profile of exo-PS H₂O solutions treated with a chelating agent (see Figure S3).

For the 1 mg/mL exo-PS solution, below the overlap concentration, the fit to the SANS data generated a Porod exponent of 3.28 ± 0.16 , consistent with a roughness or irregularity of the pores within the gel network, as illustrated by the schematic drawing in Figure 4D and supported by the SEM data at a similar length scale.

For the 5 mg/mL and 10 mg/mL exo-PS solutions, a discernable change in the q^{-n} dependency of the SANS scattering intensities is observed at q values around 0.006 Å⁻¹ and beyond, where n increases in its value (Figure 3 inset). In the case of the 1 mg/mL exo-PS solution, however, due to the poorer signal-to-noise ratio, such a transition is not as precisely defined.

The q -dependency of the SANS intensity was analyzed at various length scales for the 1 mg/mL exo-PS solution in Figure 5. The Porod region (Figure 5A) covers a q -range of approximately 0.003 Å⁻¹–0.015 Å⁻¹, corresponding to structural dimensions within the

range of $(2\pi/q) \approx 420 \text{ \AA}-2090 \text{ \AA}$. This is followed by the Lorentz region, characterized by a q -dependency of q^{-1} . The standard Kratky plot (Figure 5B) shows that at higher q ranges, the profile shifts at $q^* \approx 0.045 \text{ \AA}^{-1}$, indicating a rigid rod behavior on a local scale. At this length scale, the PS chain is expected to exhibit rigid rod-like behavior without reorientation or branching^{39,40}. The persistence length l can be calculated for an ideal Gaussian chain using the formula:

$$l = \frac{D}{q^*} \quad (3)$$

where D is a constant with a value of $6/\pi \approx 1.91$ ⁴⁰. Applying this approximation to the exo-PS polymer in this local regime, the estimated persistence length is $\approx 42 \text{ \AA}$. This length is consistent with that of three or four M2 units, suggesting a rigid rod-like behavior with no interruption between triads within each block.

Optical Microscopy, SANS, and USANS Analysis of Whole Fungal Cells.

Figure 6 and Table S2 present microscopy of *C. neoformans* H99 cells in different solutions. The microscopic images reveal a relatively high degree of variation in terms of both cell size and capsule thickness for the whole cell and gamma-irradiated cell suspensions. Without gamma irradiation, the average cell diameter was $13.9 \pm 2.9 \text{ \mu m}$ in D₂O and $13.2 \pm 3.3 \text{ \mu m}$ in H₂O, while cells subjected to gamma irradiation had an average cell diameter of $6.4 \pm 2.7 \text{ \mu m}$ in D₂O and $7.2 \pm 2.9 \text{ \mu m}$ in H₂O. The average capsule thickness before gamma-irradiation was also measured: $4.0 \pm 1.4 \text{ \mu m}$ in D₂O and $3.6 \pm 1.5 \text{ \mu m}$ in H₂O. Based on the microscopy data, the choice of solvents did not significantly affect cell diameter or capsule thickness (unpaired t-test, $P > 0.05$, ns). However, gamma irradiation removed most of the capsular-PS (unpaired t-test, $P < 0.0001$, ****).

SANS and USANS data on whole and irradiated cells are presented in Figure 7, showing good agreement between the desmeared USANS data and the SANS data. In H₂O, the scattering intensities gradually decay with increasing q both for irradiated and whole cell samples, reaching similar incoherent scattering background intensities of approximately $0.07 \text{ \AA}^{-1}-0.08 \text{ \AA}^{-1}$, dominated by contributions to incoherent scattering from the hydrogen atoms present. In contrast, D₂O samples exhibit a substantially lower incoherent neutron scattering background, allowing a discernable difference in the SANS profiles to emerge at $q > 0.1 \text{ \AA}^{-1}$. This range corresponds to the expected contribution of the M2 triads towards scattering. Notably, at these higher q values, gamma-irradiated samples display a distinct profile with a decrease in scattering intensities. This observation is consistent with the disruption of the M2 triads that SANS detects for whole cells in D₂O, but not in H₂O where it was observed that the exo-PS scattering length density is matched out. Differences are also evident in the Kratky plots for samples measured in D₂O, as present in Figure S5 in the supporting information.

Given the high polydispersity of the samples, USANS data fitting was not attempted, as neutron scattering probes a significant amount of bulk sample compared to the images in Figure 6. Additionally, unknown contributions to the scattering profile from cellular

components such as the nucleus or the cell wall further complicate data fitting. The difference in size between whole and gamma-irradiated cells is apparent from the USANS profiles for both H₂O and D₂O samples, where the scattering profiles show a maximum intensity plateau at $q < 0.00005 \text{ \AA}^{-1}$, as the intensities reach the Guinier regime. The calculated radii of gyration for irradiated cell samples, derived from Guinier analysis (Figure S4 and Table S3), are consistent with the dimensions observed by optical microscopy. For non-irradiated samples, insufficient data points were collected in the Guinier regime, preventing an unambiguous calculation of the corresponding larger cell radii of gyration.

Since exo-PS in H₂O solutions did not exhibit measurable contrast in the SANS regime, even at concentrations of 10 mg/mL, the discernible discrepancies in cell size between whole and gamma-irradiated cells in H₂O indicate differentiation between the exo-PS and capsular-PS. This is consistent with a gradient of PS densities in the pristine whole cells, ranging from an outer, more hydrated layer to an inner, denser layer closer to the cell wall, which is less solvent accessible and more resistant to ablation²³.

In the USANS data for H₂O solutions, there is an inflection point at $q \approx 0.0001 \text{ \AA}^{-1}$ that is absent in the samples containing D₂O. Considering that no significant increase in polydispersity was detected by optical microscopy for the samples in D₂O compared to H₂O, the absence of inflection in D₂O solutions is not consistent with a resolution effect. Instead, the data may reflect a structural characteristic of the fungal cell body for which the solutions in H₂O provide better SLD contrast. Given the complexity of the fungal cell and the unknown SLD of the different cell components, no specific structure or organelle can be objectively assigned to this area of the USANS profile.

Fractal Analysis of Scanning Electron Micrographs.

Image analysis of encapsulated whole cells and capsular structures reveals fractal patterns with dimensions ranging from 1.6 to 1.85 (Figure 8). Despite these samples undergoing dehydration during SEM processing and thus not being in their native state, the presence of fractal patterns in the polysaccharides is consistent with the neutron scattering data in solution. Moreover, this fractal pattern was observed even after capsule dehydration and the coalescing of PS molecules into thick fibrils. This suggests a connection between the hydrated and dehydrated structures of polysaccharides, possibly reflecting a residual capsular resistance to dehydrating conditions.

CONCLUSIONS

This study demonstrates the effective use of neutron scattering and different neutron scattering contrasts (utilizing solutions with 0% and 100% D₂O) to gain insights into the structural characteristics of both *C. neoformans* exo-PS and cells under their native conditions. Our findings present compelling evidence that exo-PS inherently exhibits mass fractal characteristics, representing a self-similar branched system or network spanning a wide range of size scales. While the presence of fractals in certain polysaccharides is not uncommon, the specific characteristics of these fractals, such as fractal dimension, can vary widely due to multiple factors, such as molecular composition, surrounding environment, and processing conditions^{6,22}.

The SANS results from exo-PS scattering are consistent with a collapsed chain-like behavior stabilized by interchain and intrachain interactions, including divalent cation bridges between negatively charged glucuronic acid residues, a phenomenon previously reported in the presence of water molecules²⁵. Future SANS and USANS studies should address the concentration effects of exo-PS on hydrogen-to-deuterium exchange levels and buffer accessibility (including chelating agents if used to further investigate the role of cation bridging in the structuring of the polysaccharide). High concentrations are likely to impact solvent buffer accessibility to the polysaccharide, while lower concentrations may favor more uniformly chain-hydrated states and minimize scattering effects arising from overlapping and entanglement.

The observed rigid rod behavior of exo-PS at local scales, with an estimated persistence length of approximately 42 Å, suggests that the arrangement of three to four GXM triads, particularly the M2 motif, involves short repeats where the chain direction may change at the end of each repeat, resulting in an overall semi-flexible structure. This local-scale rigidity of exo-PS agrees with molecular modeling studies, which propose that, at least within six GXM motifs, the ends of the chain do not bend into close proximity⁴¹.

As a dominant virulence factor often targeted for antibody treatment, exo-PS plays a crucial role in infection. Recent research has identified deca-saccharide (serotype A) as a possible minimal size for effective neutralizing mAb recognition, but our data offer a broader range of oligosaccharide sizes suitable for testing immune responses⁴². To better characterize the exo-PS secreted in humans during infection, similar studies on exo-PS secreted by isolated infecting fungal cells cultured in media with the cation compositions of human fluids should be conducted to explore the effects of different types and concentrations of counterions.

It is important to note that sample preparation protocols can influence the measured structural properties, as previously suggested¹⁰. The experimental data reflects only the structural features of the selected sample and it is likely that the parameters measured here would vary with different types of preparations. Varying molar mass cutoffs during filtration can result in significant differences in the USANS regime (data not shown) and previous studies have shown that *C. neoformans* GXM fractions of different molar masses are functionally distinct⁴³. Further work is needed to systematically characterize USANS and microscopy data for exo-PS chains representing the range of molar masses found *in vivo*. Lastly, future SANS studies could utilize isotope-labeled dextrose or specific precursors to enhance the contributions of capsular-PS to the overall scattering profiles measured from whole cells, with the goal of further elucidating the differences between capsular-PS and exo-PS¹⁰.

In summary, the application of neutron scattering to *C. neoformans* polysaccharide provides important new insights into its structure, including evidence for a fractal-like structure arising from intermolecular interactions of semi-rigid PS segments. This arrangement forms a mesh that emerges as the capsular structure observable in the macromolecular world. This in turn raises the exciting possibility that the capsule emerges from perhaps a few local interactions between polysaccharide molecules, guided by specific local rules, resulting in the magnificence that is the visible *cryptococcal* capsule. The capsule is a highly

hydrated structure that is difficult to study directly using available techniques. Therefore, our understanding of the capsule is derived from synthesizing information gathered from techniques at differing scales, spanning from microscopic observations to neutron scattering and the chemistry of the individual sugars, in the creation of testable models. In this regard, the addition of neutron scattering to the methodologies used for studying *cryptococcal* polysaccharide introduces a new and welcomed analytical tool.

Supplementary Material

Refer to Web version on PubMed Central for supplementary material.

ACKNOWLEDGMENT

This work benefited from the use of the SasView application, originally developed under NSF award DMR-0520547. SasView contains code developed with funding from the European Union's Horizon 2020 research and innovation program under the SINE2020 project, grant agreement No 654000. SCMT is grateful for funding from the cooperative agreement #70NANB20H133 from NIST, U.S. Department of Commerce. We acknowledge the support of the National Institute of Standards and Technology, U.S. Department of Commerce, in providing the neutron research facilities used in this work. This work utilized facilities supported in part by the National Science Foundation under Agreement No. DMR-0944772. Certain commercial equipment, software, instruments, and materials are identified to foster understanding. Such identification does not imply recommendation or endorsement by the National Institute of Standards and Technology, nor does it imply that the materials or equipment identified are necessarily the best available for the purpose. The statements, findings, conclusions, and recommendations are those of the authors and do not necessarily reflect the view of NIST or the U.S. Department of Commerce. RJBC was supported by the Johns Hopkins University Center for AIDS Research (P30AI094189). The authors also thank Dr. Scott A. McConnell for reviewing the data and providing valuable input.

ABBREVIATIONS

PS	polysaccharide
GXM	Glucuronoxylomannans
SANS	small-angle neutron scattering
USANS	ultra-small-angle neutron scattering
SEM	scanning electron microscopy
SLD	scattering length density

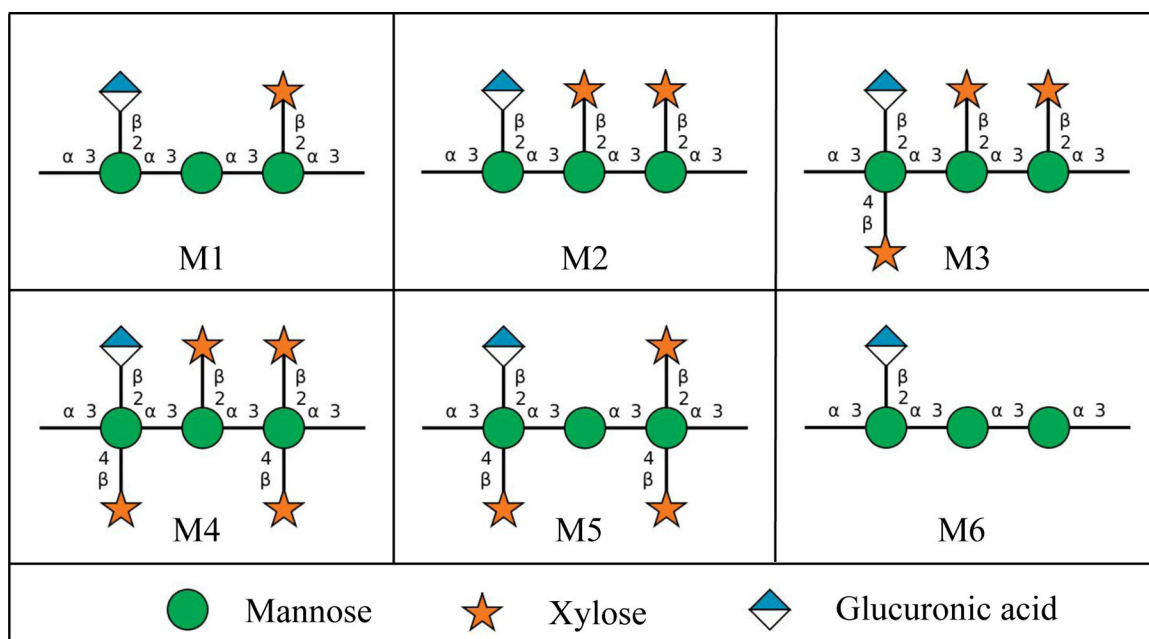
REFERENCES

- (1). Rajasingham R; Smith RM; Park BJ; Jarvis JN; Govender NP; Chiller TM; Denning DW; Loyse A; Boulware DR Global Burden of Disease of HIV-Associated Cryptococcal Meningitis: An Updated Analysis. *Lancet Infect. Dis* 2017, 17 (8), 873–881. 10.1016/s1473-3099(17)30243-8. [PubMed: 28483415]
- (2). Ngan NTT; Flower B; Day JN Treatment of Cryptococcal Meningitis: How Have We Got Here and Where Are We Going? *Drugs* 2022, 82 (12), 1237–1249. 10.1007/s40265-022-01757-5. [PubMed: 36112342]
- (3). Pappas PG; Perfect JR; Cloud GA; Larsen RA; Pankey GA; Lancaster DJ; Henderson H; Kauffman CA; Haas DW; Saccente M; Hamill RJ; Holloway MS; Warren RM; Dismukes WE Cryptococcosis in Human Immunodeficiency Virus-Negative Patients in the Era of Effective Azole Therapy. *Clin. Infect. Dis* 2001, 33 (5), 690–699. 10.1086/322597. [PubMed: 11477526]

- (4). Casadevall A; Coelho C; Cordero RJB; Dragotakes Q; Jung E; Vij R; Wear MP The Capsule of *Cryptococcus Neoformans*. *Virulence* 2019, 10 (1), 822–831. 10.1080/21505594.2018.1431087. [PubMed: 29436899]
- (5). Maxson ME; Cook E; Casadevall A; Zaragoza O The Volume and Hydration of the *Cryptococcus Neoformans* Polysaccharide Capsule. *Fungal Genet. Biol* 2007, 44 (3), 180–186. 10.1016/j.fgb.2006.07.010. [PubMed: 16963294]
- (6). Wear MP; Hargett AA; Kelly JE; McConnell SA; Crawford CJ; Freedberg DI; Stark RE; Casadevall A Lyophilization Induces Physicochemical Alterations in Cryptococcal Exopolysaccharide. *Carbohydr. Polym* 2022, 291, 119547. 10.1016/j.carbpol.2022.119547. [PubMed: 35698377]
- (7). Cordero RJB; Pontes B; Frases S; Nakouzi AS; Nimrichter L; Rodrigues ML; Viana NB; Casadevall A Antibody Binding to *Cryptococcus Neoformans* Impairs Budding by Altering Capsular Mechanical Properties. *J. Immunol* 2013, 190 (1), 317–323. 10.4049/jimmunol.1202324. [PubMed: 23233725]
- (8). Bowen A; Wear MP; Cordero RJB; Oscarson S; Casadevall A A Monoclonal Antibody to *Cryptococcus Neoformans* Glucuronoxylomannan Manifests Hydrolytic Activity for Both Peptides and Polysaccharides*. *J. Biol. Chem* 2017, 292 (2), 417–434. 10.1074/jbc.m116.767582. [PubMed: 27872188]
- (9). Cordero RJB; Pontes B; Guimarães AJ; Martinez LR; Rivera J; Fries BC; Nimrichter L; Rodrigues ML; Viana NB; Casadevall A Chronological Aging Is Associated with Biophysical and Chemical Changes in the Capsule of *Cryptococcus Neoformans*. *Infect. Immun* 2011, 79 (12), 4990–5000. 10.1128/iai.05789-11. [PubMed: 21968999]
- (10). Frases S; Nimrichter L; Viana NB; Nakouzi A; Casadevall A *Cryptococcus Neoformans* Capsular Polysaccharide and Exopolysaccharide Fractions Manifest Physical, Chemical, and Antigenic Differences. *Eukaryot. cell* 2007, 7 (2), 319–327. 10.1128/ec.00378-07. [PubMed: 18156290]
- (11). Frases S; Pontes B; Nimrichter L; Rodrigues ML; Viana NB; Casadevall A The Elastic Properties of the *Cryptococcus Neoformans* Capsule. *Biophys. J* 2009, 97 (4), 937–945. 10.1016/j.bpj.2009.04.043. [PubMed: 19686640]
- (12). Fonseca FL; Nohara LL; Cordero RJB; Frases S; Casadevall A; Almeida IC; Nimrichter L; Rodrigues ML Immunomodulatory Effects of Serotype B Glucuronoxylomannan from *Cryptococcus Gattii* Correlate with Polysaccharide Diameter. *Infect. Immun* 2010, 78 (9), 3861–3870. 10.1128/iai.00111-10. [PubMed: 20547742]
- (13). Cordero RJB; Frases S; Guimarães AJ; Rivera J; Casadevall A Evidence for Branching in Cryptococcal Capsular Polysaccharides and Consequences on Its Biological Activity. *Mol. Microbiol* 2011, 79 (4), 1101–1117. 10.1111/j.1365-2958.2010.07511.x. [PubMed: 21208301]
- (14). Ellerbroek PM; Lefeber DJ; Veghel R. van; Scharringa J; Brouwer E; Gerwig GJ; Janbon G; Hoepelman AIM; Coenjaerts FEJ O-Acetylation of Cryptococcal Capsular Glucuronoxylomannan Is Essential for Interference with Neutrophil Migration. *J. Immunol* 2004, 173 (12), 7513–7520. 10.4049/jimmunol.173.12.7513. [PubMed: 15585878]
- (15). Belay T; Cherniak R; Kozel TR; Casadevall A Reactivity Patterns and Epitope Specificities of Anti-*Cryptococcus Neoformans* Monoclonal Antibodies by Enzyme-Linked Immunosorbent Assay and Dot Enzyme Assay. *Infect. Immun* 1997, 65 (2), 718–728. 10.1128/iai.65.2.718-728.1997. [PubMed: 9009335]
- (16). Frases S; Pontes B; Nimrichter L; Viana NB; Rodrigues ML; Casadevall A Capsule of *Cryptococcus Neoformans* Grows by Enlargement of Polysaccharide Molecules. *Proc. Natl. Acad. Sci* 2009, 106 (4), 1228–1233. 10.1073/pnas.0808995106. [PubMed: 19164571]
- (17). McFadden DC; Fries BC; Wang F; Casadevall A Capsule Structural Heterogeneity and Antigenic Variation in *Cryptococcus Neoformans*. *Eukaryot. Cell* 2007, 6 (8), 1464–1473. 10.1128/ec.00162-07. [PubMed: 17601878]
- (18). Casadevall A; Nakouzi A; Crippa PR; Eisner M Fungal Melanins Differ in Planar Stacking Distances. *PLoS ONE* 2012, 7 (2), e30299. 10.1371/journal.pone.0030299. [PubMed: 22359541]
- (19). Cherniak R; Valafar H; Morris LC; Valafar F *Cryptococcus Neoformans* Chemotyping by Quantitative Analysis of ¹H Nuclear Magnetic Resonance Spectra of Glucuronoxylomannans with a Computer-Simulated Artificial Neural Network. *Clin. Diagn. Lab. Immunol* 1998, 5 (2), 146–159. 10.1128/cdli.5.2.146-159.1998. [PubMed: 9521136]

- (20). Nakouzi A; Zhang T; Oscarson S; Casadevall A The Common Cryptococcus Neoformans Glucuronoxylomannan M2 Motif Elicits Non-Protective Antibodies. *Vaccine* 2009, 27 (27), 3513–3518. 10.1016/j.vaccine.2009.03.089. [PubMed: 19464529]
- (21). Cheng K; Zhou Y; Neelamegham S Drawglycan-SNFG: A Robust Tool to Render Glycans and Glycopeptides with Fragmentation Information. *Glycobiology* 2017, 27 (3), 200–205. 10.1093/glycob/cww115. [PubMed: 28177454]
- (22). Yu L; Yakubov GE; Gilbert EP; Sewell K; van de Meene AML; Stokes JR Multi-Scale Assembly of Hydrogels Formed by Highly Branched Arabinoxylans from *Plantago Ovata* Seed Mucilage Studied by USANS/SANS and Rheology. *Carbohydr. Polym* 2019, 207, 333–342. 10.1016/j.carbpol.2018.11.098. [PubMed: 30600014]
- (23). Maxson ME; Dadachova E; Casadevall A; Zaragoza O Radial Mass Density, Charge, and Epitope Distribution in the *Cryptococcus Neoformans* Capsule. *Eukaryot. Cell* 2007, 6 (1), 95–109. 10.1128/ec.00306-06. [PubMed: 17114596]
- (24). Bryan RA; Zaragoza O; Zhang T; Ortiz G; Casadevall A; Dadachova E Radiological Studies Reveal Radial Differences in the Architecture of the Polysaccharide Capsule of *Cryptococcus Neoformans*. *Eukaryot. Cell* 2005, 4 (2), 465–475. 10.1128/ec.4.2.465-475.2005. [PubMed: 15701808]
- (25). Nimrichter L; Frases S; Cinelli LP; Viana NB; Nakouzi A; Travassos LR; Casadevall A; Rodrigues ML Self-Aggregation of *Cryptococcus Neoformans* Capsular Glucuronoxylomannan Is Dependent on Divalent Cations. *Eukaryot. cell* 2007, 6 (8), 1400–1410. 10.1128/ec.00122-07. [PubMed: 17573547]
- (26). Masuko T; Minami A; Iwasaki N; Majima T; Nishimura S-I; Lee YC Carbohydrate Analysis by a Phenol–Sulfuric Acid Method in Microplate Format. *Anal. Biochem* 2005, 339 (1), 69–72. 10.1016/j.ab.2004.12.001. [PubMed: 15766712]
- (27). Vadillo DC; Mathues W; Clasen C Microsecond Relaxation Processes in Shear and Extensional Flows of Weakly Elastic Polymer Solutions. *Rheol. Acta* 2012, 51 (8), 755–769. 10.1007/s00397-012-0640-z.
- (28). Ying Q; Chu B Overlap Concentration of Macromolecules in Solution. *Macromolecules* 1987, 20 (2), 362–366. 10.1021/ma00168a023.
- (29). Glinka CJ; Barker JG; Hammouda B; Krueger S; Moyer JJ; Orts WJ The 30 m Small-Angle Neutron Scattering Instruments at the National Institute of Standards and Technology. *J. Appl. Crystallogr* 1998, 31 (3), 430–445. 10.1107/s0021889897017020.
- (30). Barker JG; Glinka CJ; Moyer JJ; Kim MH; Drews AR; Agamalian M Design and Performance of a Thermal-Neutron Double-Crystal Diffractometer for USANS at NIST. *J. Appl. Crystallogr* 2005, 38 (6), 1004–1011. 10.1107/s0021889805032103.
- (31). Kline SR Reduction and Analysis of SANS and USANS Data Using IGOR Pro. *J. Appl. Crystallogr* 2006, 39 (6), 895–900. 10.1107/s0021889806035059.
- (32). Hammouda B; Ho DL; Kline S Insight into Clustering in Poly(Ethylene Oxide) Solutions. *Macromolecules* 2004, 37 (18), 6932–6937. 10.1021/ma049623d.
- (33). Gilbert EP Small-angle X-ray and Neutron Scattering in Food Colloids. *Curr. Opin. Colloid Interface Sci* 2019, 42, 55–72. 10.1016/j.cocis.2019.03.005.
- (34). Jaksch S; Pipich V; Frielinghaus H Multiple Scattering and Resolution Effects in Small-Angle Neutron Scattering Experiments Calculated and Corrected by the Software Package Muscatt. *J. Appl. Crystallogr* 2021, 54 (6), 1580–1593. 10.1107/S1600576721009067. [PubMed: 34963761]
- (35). Hyland LL; Taraban MB; Hammouda B; Yu YB Mutually Reinforced Multicomponent Polysaccharide Networks. *Biopolymers* 2011, 95 (12), 840–851. 10.1002/bip.21687. [PubMed: 21698596]
- (36). Muller F; Manet S; Jean B; Chambat G; Boué F; Heux L; Cousin F SANS Measurements of Semiflexible Xyloglucan Polysaccharide Chains in Water Reveal Their Self-Avoiding Statistics. *Biomacromolecules* 2011, 12 (9), 3330–3336. 10.1021/bm200881x. [PubMed: 21806009]
- (37). McFadden D; Zaragoza O; Casadevall A The Capsular Dynamics of *Cryptococcus Neoformans*. *Trends Microbiol* 2006, 14 (11), 497–505. 10.1016/j.tim.2006.09.003. [PubMed: 16996739]
- (38). GLYCAM-Web | Utilities for molecular modeling of carbohydrates Woods Group. <http://glycam.org> (accessed 2023-11-01).

- (39). Rosales AM; Murnen HK; Kline SR; Zuckermann RN; Segalman RA Determination of the Persistence Length of Helical and Non-Helical Polypeptoids in Solution. *Soft Matter* 2012, 8 (13), 3673–3680. 10.1039/c2sm07092h.
- (40). Gupta AK; Cotton JP; Marchal E; Burchard W; Benoit H Persistence Length of Cellulose Tricarbanilate by Small-Angle Neutron Scattering. *Polymer* 1976, 17 (5), 363–366. 10.1016/0032-3861(76)90228-7.
- (41). Kuttel MM; Casadevall A; Oscarson S Cryptococcus Neoformans Capsular GXM Conformation and Epitope Presentation: A Molecular Modelling Study. *Molecules* 2020, 25 (11), 2651. 10.3390/molecules25112651. [PubMed: 32517333]
- (42). Guazzelli L; Crawford CJ; Ulc R; Bowen A; McCabe O; Jedlicka AJ; Wear MP; Casadevall A; Oscarson S A Synthetic Glycan Array Containing Cryptococcus Neoformans Glucuronoxylomannan Capsular Polysaccharide Fragments Allows the Mapping of Protective Epitopes. *Chem. Sci* 2020, 11 (34), 9209–9217. 10.1039/d0sc01249a. [PubMed: 34123169]
- (43). Albuquerque PC; Fonseca FL; Dutra FF; Bozza MT; Frases S; Casadevall A; Rodrigues ML Cryptococcus Neoformans Glucuronoxylomannan Fractions of Different Molecular Masses Are Functionally Distinct. *Futur. Microbiol* 2014, 9 (2), 147–161. 10.2217/fmb.13.163.

**Figure 1.**

The six Glucuronoxylomannan (GXM) motifs that build up fungal exo-PS and capsular-PS. GXM is composed of a combination of six repeating units (M1-6), defined by a glucuronic acid (GlcA) residue every 3rd mannose with varying xylose substitutions. These 6 motifs of GXM in various combinations correlate to different serotype activities¹⁹. *C. neoformans* H99 serotype A has a dominant M2 motif in exo- and capsular-PS²⁰. Polysaccharide molecules can be heteropolymers composed of more than one triad¹⁷. Image created with DrawGlycan-SNFG²¹.

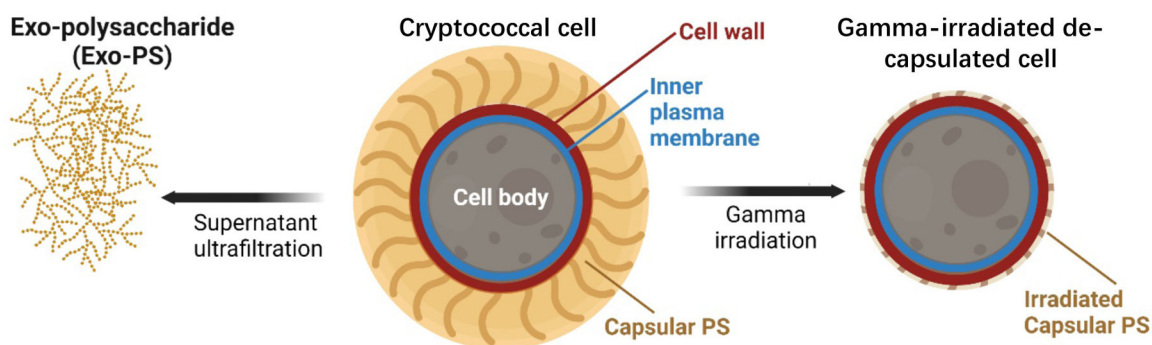


Figure 2. Schematic diagram of the samples investigated: exo-PS, *cryptococcal* cell, and gamma-irradiated de-capsulated cell. Exo-PS refers to the secreted polysaccharide, while capsular-PS refers to the highly hydrated polysaccharide surrounding the capsule of the intact cell. Gamma-irradiated capsular-PS refers to the remaining polysaccharide thin capsule surrounding the irradiated cells. Image created with [BioRender.com](https://www.biorender.com).

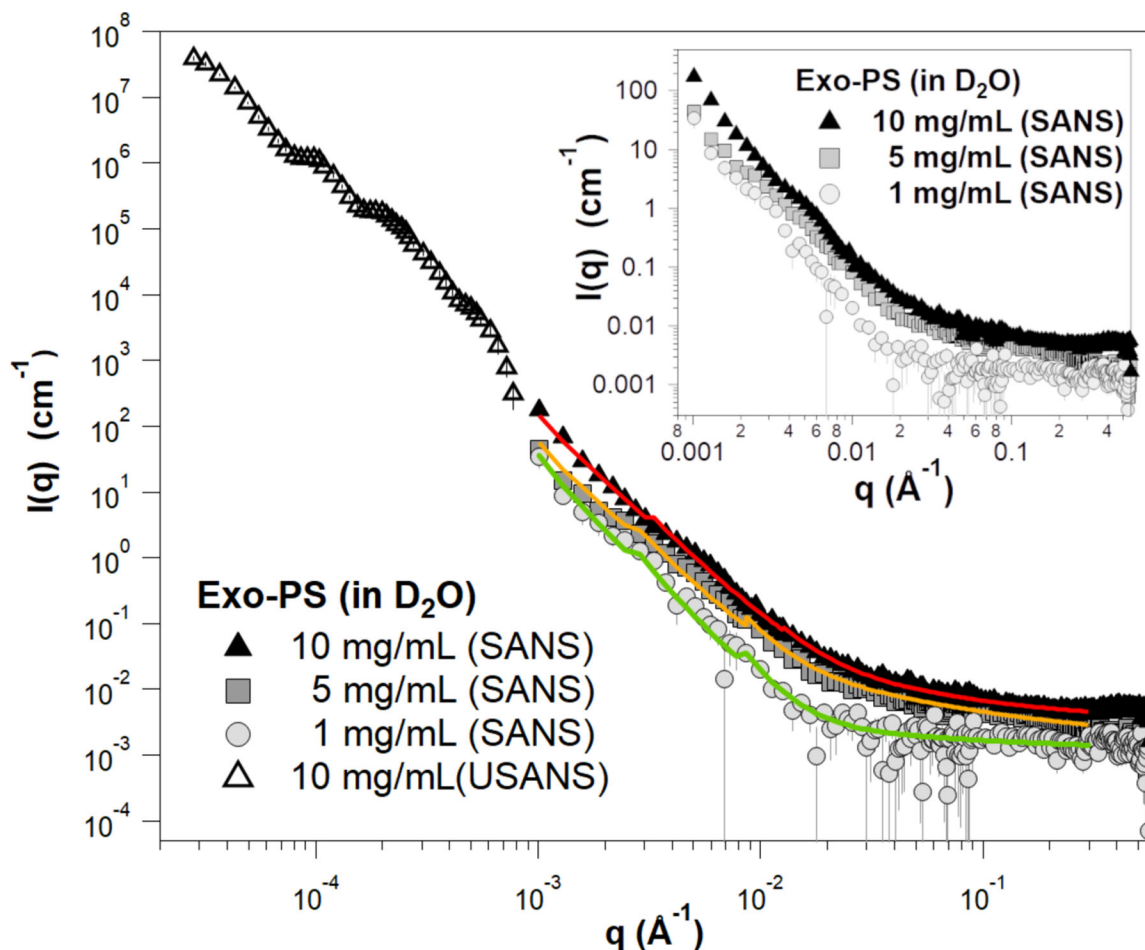


Figure 3. Background-subtracted, reduced SANS, and USANS data for the exo-PS solutions in D_2O at varying concentrations. The USANS data shown has been desmeared using the macro-routines for Igor provided by the NCNR to account for the slit-smearing effects of the BT5 instrument on the experimental data. The solid lines depict SANS data fits for the solutions at 1 mg/mL (green), 5 mg/mL (orange), and 10 mg/mL (red) exo-PS; it should be noted that the small discontinuities in the line fit at $q \approx 0.03 \text{ \AA}^{-1}$ and $q \approx 0.09 \text{ \AA}^{-1}$ are a resolution artifact related to the instrumental configurations used for data collection and are not indicative of a sample-related scattering characteristic. The inset provides an enlarged view of the SANS data to highlight the distinctions observed between different concentrations. The error bars represent standard errors derived from counting statistics and, when not visibly discernible, are smaller than the corresponding data markers.

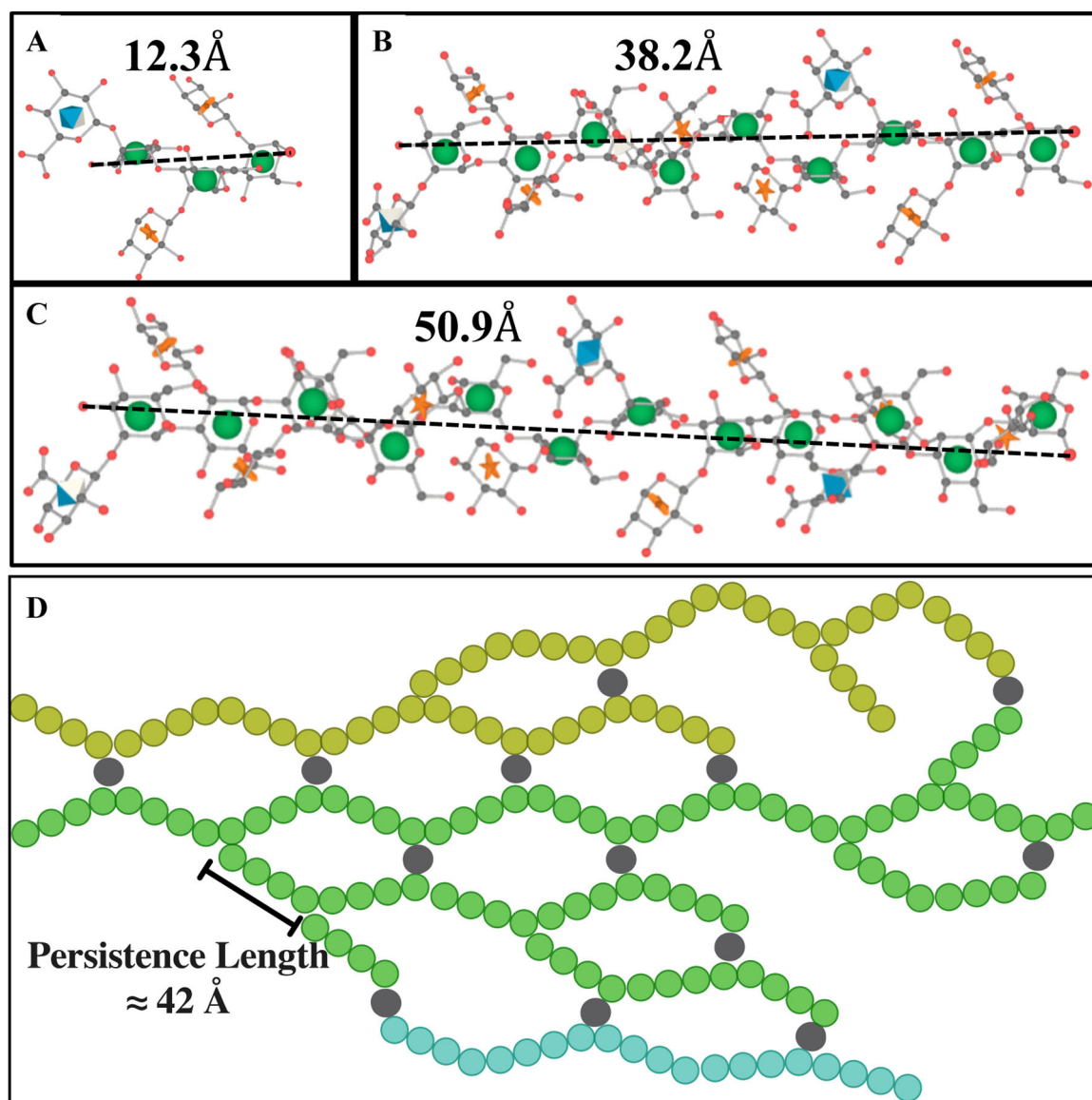


Figure 4.

Schematic representation of M2 motif and exo-PS in water for one M2 (A), three M2 (B), and four M2 (C) triads, drawn and energy minimized using GLYCAM³⁸. Residues are represented by their symbol nomenclature: green sphere for mannose, orange star for xylose, and blue diamond for GlcA. The distance between the two furthest oxygens that connect mannoses was measured to determine the approximate length of one (12.3 Å), three (38.2 Å), or four (50.9 Å) triads, respectively. (D) The exo-PS in water is drawn in 2D to suggest a compatible arrangement of the exo-PS structure, where each circle (except gray circles that represent divalent cations) represents one triad, and three exemplar chains are represented with different colors. A potential pattern of intra- and inter-chain ionic bridging by the divalent cations such as Mg²⁺ and Ca²⁺ (represented by gray circles) present in the cell culture media. The corresponding estimated persistence length (length of the region with rigid rod behavior) is approximately 42 Å. Image created with [BioRender.com](https://www.bio-render.com).

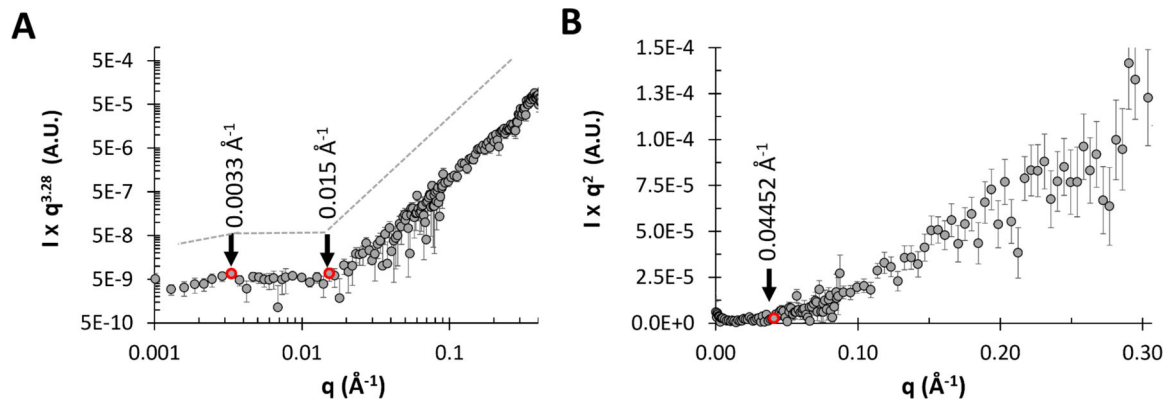


Figure 5. SANS data for 1 mg/mL exo-PS solution in D₂O, are shown as (A) Porod exponent-weighted intensities and (B) a standard Kratky plot.

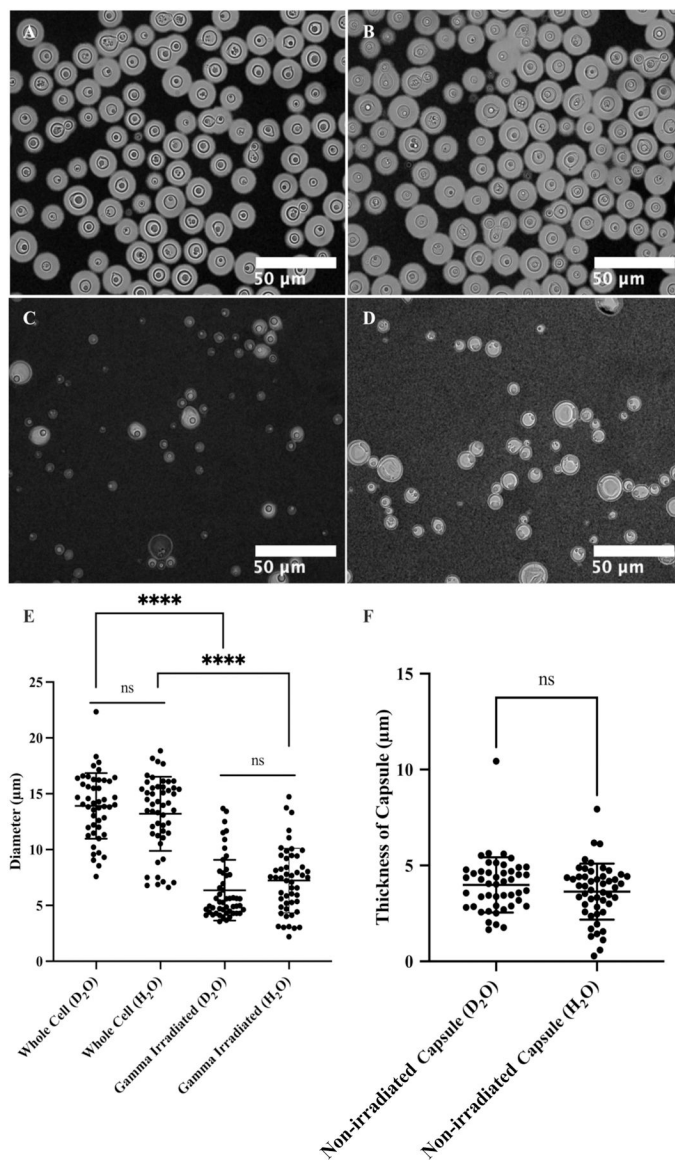


Figure 6.

Microscopy of *C. neoformans* H99 cells in water and the effect of gamma irradiation on cellular and capsular dimensions. Samples were counterstained with India Ink particles, which are excluded by the dense PS capsule. Cells without gamma irradiation were resuspended in D₂O (A) and H₂O (B), and cells treated with 40 minutes of gamma irradiation were resuspended in D₂O (C) and H₂O (D) as well. The cell diameters of all four samples were estimated (E), and capsule thickness for whole cells was obtained as the differences between the radii of cells and cell bodies (F). The t-test analyses are labeled based on their p-value (p > 0.05: ns; p < 0.05: *; p < 0.01: **; p < 0.001: ***; p < 0.0001: ****).

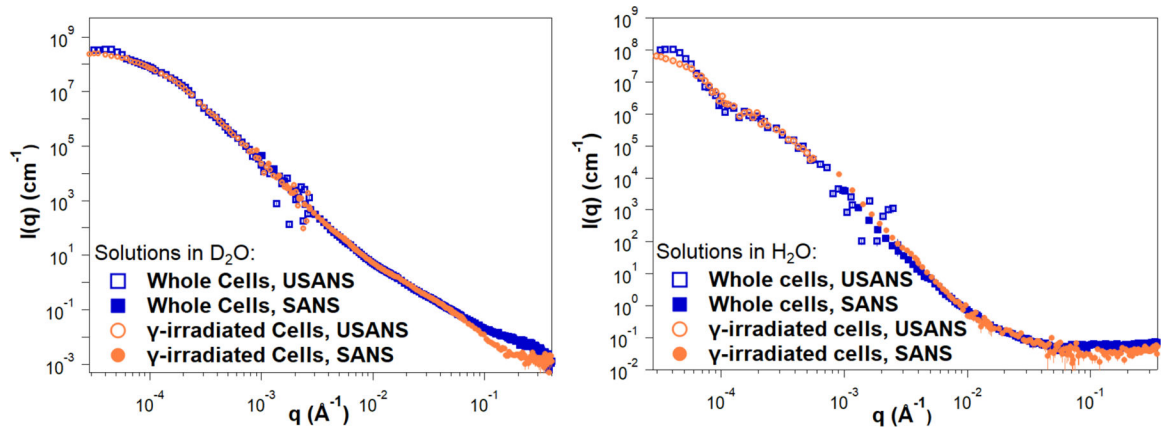


Figure 7.

Reduced SANS (buffer subtracted) and USANS data collected for fungal cells in D_2O and H_2O solutions, for both intact and gamma-irradiated cells. The desmeared USANS data displayed compensates for the slit-smearing effects on the experimental data, allowing direct comparison with the SANS data for each sample. Error bars represent standard errors from counting statistics and are smaller than the corresponding data marker when not visible.

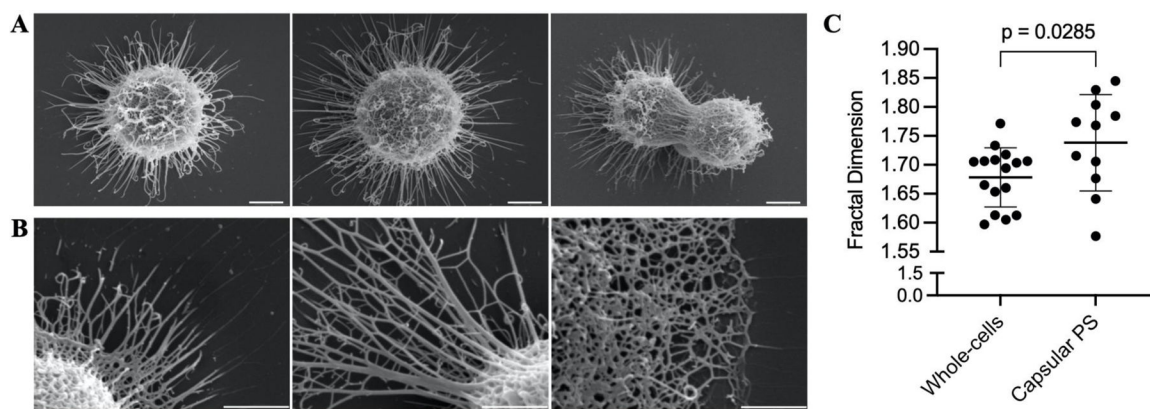


Figure 8. Fractal analysis of SEM micrographs of whole encapsulated cells and capsular-PS structures. (A) Representative whole encapsulated *C. neoformans* cells and (B) capsular-PS structures, showing the fractal structure and the presence of an irregular pore network. Scale bars represent 2 and 1 micrometers, respectively. (C) Fractal dimensions of 27 micrographs were analyzed using the FracLac plugin in ImageJ.